GENETICS

The telomerase reverse transcriptase elongates reversed replication forks at telomeric repeats

Armela Huda[1], Hiroshi Arakawa[1], Giulia Mazzucco[1], Martina Galli[1], Valentina Petrocelli[2], Stefano Casola[1], Lu Chen[3,4], Ylli Doksani[1]*

The telomerase reverse transcriptase elongates telomeres to prevent replicative senescence. This process requires exposure of the 3′-end, which is thought to occur when two sister telomeres are generated at replication completion. Using two-dimensional agarose gel electrophoresis (2D-gels) and electron microscopy, we found that telomeric repeats are hotspots for replication fork reversal. Fork reversal generates 3′ telomeric ends before replication completion. To verify whether these ends are elongated by telomerase, we probed de novo telomeric synthesis in situ and at replication intermediates by reconstituting mutant telomerase that adds a variant telomere sequence. We found variant telomeric repeats overlapping with telomeric reversed forks in 2D-gels, but not with normal forks, nontelomeric reversed forks, or telomeric reversed forks with a C-rich 3′-end. Our results define reversed telomeric forks as a substrate of telomerase during replication.

INTRODUCTION

Linear chromosomes end in several kilobases of telomeric repeats, bound by the shelterin complex, which prevents activation of a DNA damage response at chromosome ends (*1*). Telomere function is essential for cellular proliferation and chromosome stability. Gradual erosion of telomeres is counteracted by the telomerase reverse transcriptase (TERT), which uses an internal RNA template (TR) to add telomeric repeats to the 3′-ends of chromosomes (*2*). Telomere maintenance, however, depends also on faithful duplication of the bulk of repeats by the replication machinery every S phase. Several lines of evidence suggest that this task is challenging. Telomeres behave like replication fragile sites and constitutively require the action of specialized helicases to assist replication (*3*–*7*). In their absence, large fragments of telomeric repeats can be lost in a single S phase, likely due to replication failure (*3*, *6*). The severe telomere replication defects observed in shelterin mutants, from yeast to mammals, suggest that shelterin plays an essential function in assisting semiconservative replication of telomeric repeats (*4*, *8*, *9*). Several telomeric features have been invoked as potential obstacles to fork progression, including the presence of tightly bound proteins, ongoing transcription, or secondary structures like G4-DNA, t-loops, R-loops, and damage-induced i-loops (*6*, *10*–*15*). However, the relative contribution of each of these factors to telomere replication stress is not clear. Electron microscopy (EM) analysis of model replication forks has shown that the presence of TTAGGG repeats induces spontaneous fork reversal in vitro (*16*). Two-dimensional agarose gel electrophoresis (2D-gels) has revealed that replication fork pausing at yeast telomeres and fork collapse events have been observed in mutants with telomere dysfunction (*8*, *17*–*19*). In *taz1* mutants in *Schizosaccharomyces pombe*, fork collapse at telomeric repeats is associated with an increase recruitment and activity of telomerase, suggesting that collapsed telomeric forks might represent a robust substrate for telomerase (*20*). In these settings, it was found that telomerase played an important role in restoring telomere length after replication failures by synthesizing long stretches of telomeres or, possibly, by acting directly on collapsed replication forks (*8*, *19*, *20*). While in yeast telomerase activity seems to alleviate the consequences of telomere replication stress, genetic analysis of rapid telomere deletion events in mouse cells has suggested a different scenario, where telomerase loading on reversed telomeric forks would lead to replication failures, a pathological activity that is kept at bay by the Rtel1 helicase (*21*). Replication stress at mammalian telomeres is often monitored through the scars it leaves on telomere fluorescence in situ hybridization (FISH) signals on chromosome spreads. Phenotypes like fragile (decondensed) telomeres, signal heterogeneity, or telomere loss are indicative of replication failures but provide no molecular detail on the fate of telomeric forks. Differently from yeast, 2D-gel analysis of mammalian telomeric forks has not been possible so far and, overall, there is a lack of structural information on the fate of telomeric forks in mammalian cells.

To overcome these limitations, we have monitored by 2D-gels and EM the structure of replication forks traveling through long stretches of telomeric repeats, introduced into a Simian virus 40 (SV40) mini-chromosome. We found that replication of telomeric repeats is characterized by an increased frequency of replication fork reversal, which occurred in a length-dependent but orientation-independent fashion. In agreement with this result, EM analysis of enriched mouse telomeres revealed accumulation of reversed forks also at endogenous telomeric repeats, when compared with the bulk DNA of the same sample. To probe the activity of telomerase at stalled telomeric forks, we expressed a mutated telomerase TR, *hTR-TSQ1* (tolerated sequence 1), which introduces GTTGCG repeats, in cells with the SV40 mini-chromosome containing telomeric repeats (*22*). 2D-gel analysis, combined with specific probes, revealed the addition of TSQ1 repeats specifically on

[1]IFOM ETS-The AIRC Institute of Molecular Oncology, Milan, Italy. [2]Institute for Tumor Biology and Experimental Therapy, Frankfurt Cancer Institute, Goethe University Frankfurt, Frankfurt am Main, Germany. [3]Nuclear Dynamics and Cancer Program, Cancer Epigenetics Institute, Fox Chase Cancer Center, Philadelphia, PA, USA [4]Department of Cancer and Cellular Biology, Lewis Katz School of Medicine, Temple University, Philadelphia, PA, USA.
*Corresponding author. Email: ylli.doksani@ifom.eu

molecules that migrate as reversed forks, in the cone signal. No signal was detected at normal replication forks, at nontelomeric reversed forks, or at telomeric reversed forks with a C-rich 3′-end. Our results estimate a nearly twofold increase in the probability of replication fork reversal at telomeric repeats compared to the rest of the genome. We show that reversed telomeric forks generate a 3′-end that is elongated by the TERT in vivo. These results reveal another substrate for telomerase, which is generated before the completion of chromosome replication. Our results also suggest the existence of replisome-associated factors that control telomerase activity during telomere replication, similar to what has been proposed for Rtel1 (*21*). Frequent fork reversal would result in the generation of free telomeric ends during replication that, if left unresolved or unprotected, could be engaged in aberrant DNA repair, resulting in telomere dysfunction and genome instability.

RESULTS

Replication fork reversal at telomeric repeats in an SV40 mini-chromosome

To monitor the structure of replication forks traveling through telomeric repeats, we used an SV40 mini-chromosome–based system, previously used to study other repetitive elements in human cells (*23*). A stretch of 115 telomeric repeats was inserted next to the SV40 origin of replication in both orientations (Fig. 1A). The constructs were transfected in human embryonic kidney (HEK)–293T cells where they undergo replication, and 40 hours after transfection, the SV40 mini-chromosomes were extracted following precipitation of intact genomic DNA in high salt, according to the Hirt procedure (*24*). These constructs are chromatinized in vivo (*23*), and consistent with previous work showing binding of shelterin components on telomeric repeats in episomal constructs (*25*), we found that TRF1 is recruited at the telomeric repeats on the SV40 mini-chromosome (Fig. 1B and fig. S1A). When equal amounts of a construct with 115 telomeric repeats and a nontelomeric control of equal length were cotransfected and allowed to replicate, we recovered around 30% less of the former, suggesting an increased incidence of replication failure at telomeric repeats (fig. S1, B and C). We monitored by neutral 2D-gel electrophoresis the structure of replication forks arising from the SV40 origin and moving through the telomeric repeats. To prevent branch migration of replication intermediates, the DNA was psoralen–cross-linked in vivo, before extraction (*26*). A 5.26-kb Bam HI–Sac I restriction fragment, containing the SV40 origin and the telomeric insert, was separated

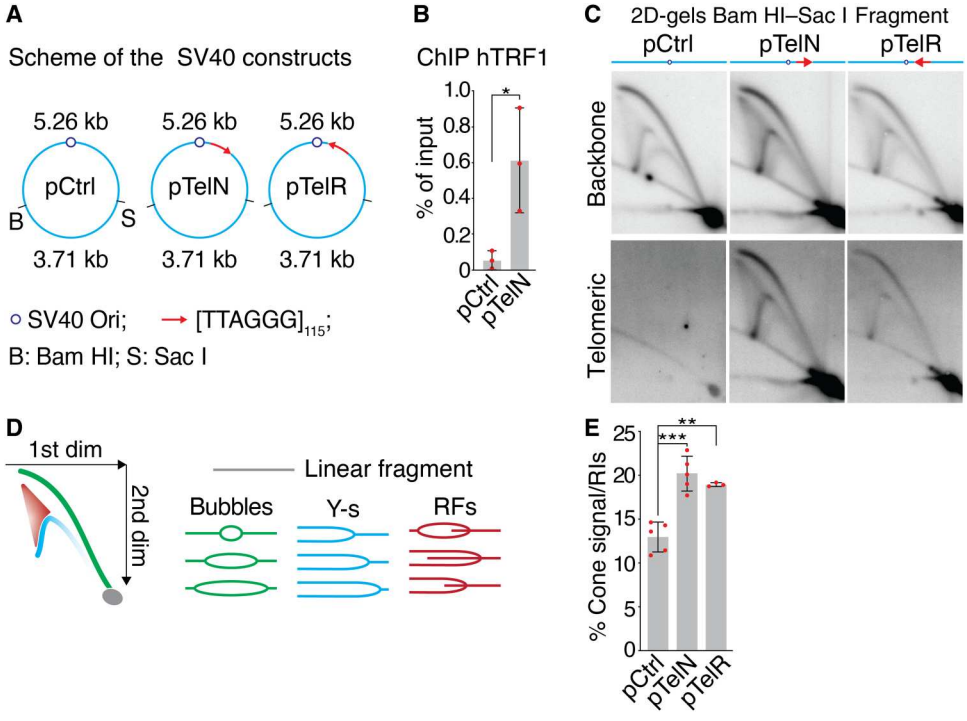

Fig. 1. Replication fork reversal at telomeric repeats on the SV40 mini-chromosome. (**A**) Schematic representation of the SV40 constructs used in this study. The Bam HI–Sac I restriction sites are shown. (**B**) Chromatin immunoprecipitation (ChIP) analysis showing loading of the shelterin component TRF1 to ectopic telomeric repeats on the pTelN construct (see also fig. S1A). HEK-293T cells were transfected with the indicated constructs, allowed to replicate, collected 40 hours after transfection, and processed for ChIP with an anti-hTRF1 antibody. Bars show mean with SD from three independent experiments. The *P* value was derived from an unpaired, two-tailed Student's *t* test. (**C**) 2D-gels showing the accumulation of the cone signal in the constructs with telomeric repeats (see also fig. S1D). HEK-293T cells were transfected with the constructs indicated in (A), allowed to replicate, collected 40 hours after transfection, and psoralen–cross-linked in vivo. Then, extra-chromosomal DNA was extracted with the Hirt procedure; digested with Bam HI, Sac I, and Dpn I (to remove unreplicated plasmids); and separated in 2D-gels. The gels were blotted into a membrane and hybridized with a ^{32}P-labeled Bam HI–Sac I 4.53-kb fragment from the pML113 construct (backbone) (top); then, the membrane was stripped and hybridized with a probe recognizing the telomeric repeats (telomeric) (bottom). (**D**) Schematic representation of the 2D-gel migration profile of the indicated DNA replication intermediates. Note that the distinct pattern, generated by each class of intermediates, is color-coded. (**E**) Quantification of the cone signal expressed as a percentage of all replication intermediates from three to five independent experiments as the one shown in (C). Bars show mean with SD. *P* values derived from unpaired, two-tailed Student's *t* test.

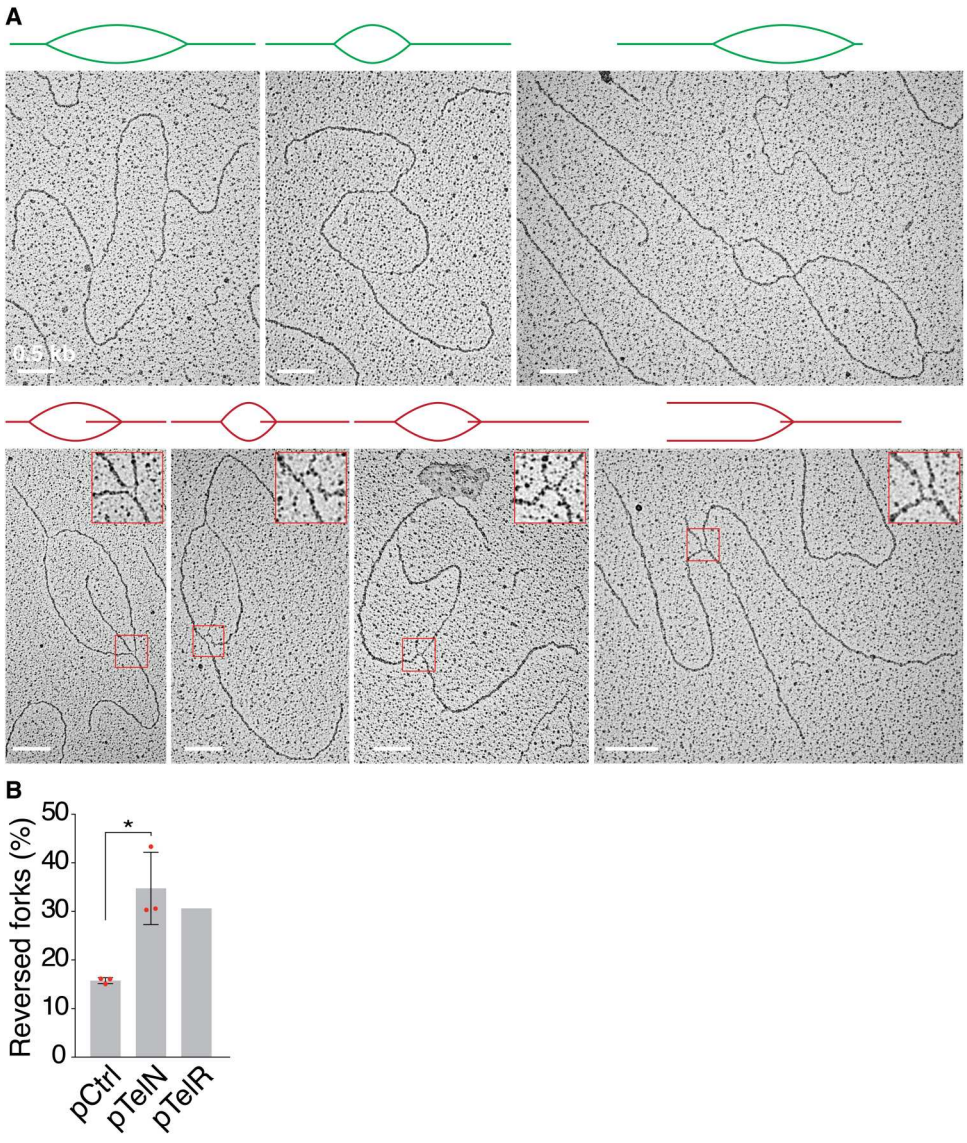

Fig. 2. Fork reversal at the ectopic telomeric repeats, visualized by electron microscopy. (**A**) Representative EM images of normal replication bubbles (top), replication bubbles with fork reversal, and an X-shaped intermediate compatible with fork reversal, in the pTelN construct. The DNA, derived from an identical experimental procedure as the one in Fig. 1C, was digested with Bam HI and Sac I, and the replication intermediates were purified from an agarose gel (see also fig. S2). The samples were spread and visualized in EM. A scheme of the molecule visualized is shown above each image. Inset shows a magnification of the area inside the red square. Scale bars, 180 nm (0.5 kb). (**B**) Quantification of the percentage of molecules compatible with a reversed fork structure, over all replication forks from three independent experiments as the one shown in (A) for pTelN and pCtrl and one experiment for pTelR. *N* = 157, 60, and 320 and 124, 56, and 166 replication forks for pTelN and pCtrl, respectively, and 76 forks for pTelR. Bars represent mean with SD. The *P* value was derived from unpaired, two-tailed Student's *t* test.

in 2D-gels (Fig. 1, A, C, and D). All constructs accumulated bubbles and large Y-s, indicating that the nearby telomeric repeats do not affect SV40 origin activity (Fig. 1, C and D). No obvious pausing spots were visible in 2D-gels in the fragment with the telomeric repeats (see below). The telomeric sample showed a more intense cone signal (Fig. 1, C to E). This signal is generated by X-shaped DNA structures associated with replication fork reversal (*27*–*29*). While the cone signal accumulated in the construct with 115 telomeric repeats, constructs with 34 or 54 repeats did not show a consistent increase in cone signal intensity (fig. S1, D and E). The cone signal accumulated both in the pTelN construct (where the G-rich parental strand is replicated as the lagging strand) and in the pTelR construct with reversed orientation (where the C-rich parental strand is replicated as the lagging strand), arguing against the formation of G4-DNA as the main cause of fork reversal in this setting (Fig. 1, C to E). Consistently, treatment with the G4 ligand pyridostatin did not result in a further accumulation of reversed forks in the sample with the telomeric repeats (fig. S1, F and G). These results suggest an increased incidence of replication fork reversal at telomeric repeats in the SV40 mini-chromosome, which occurs in a length-dependent and orientation-independent manner.

To corroborate these findings, replication forks within the same 5.26-kb Bam HI–Sac I restriction fragment analyzed above were spread and visualized by EM. For this type of analysis, replicating

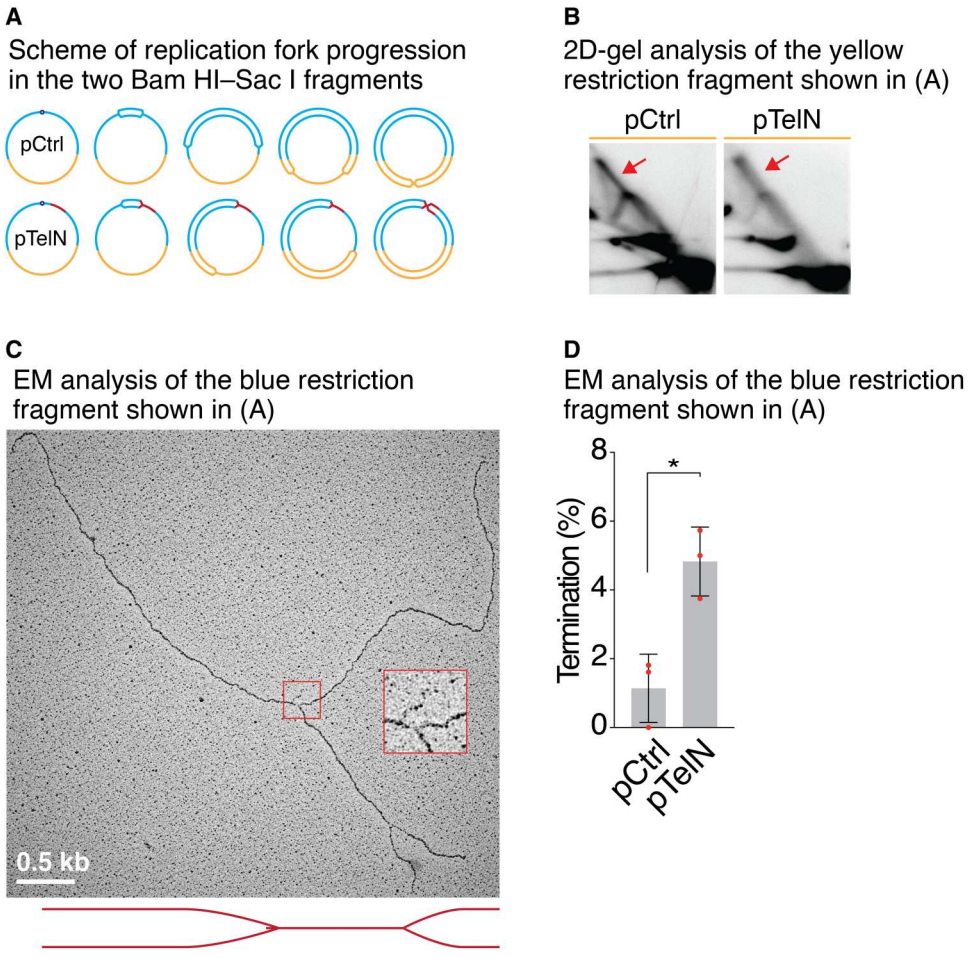

Fig. 3. Fork stalling and termination at the telomeric repeats in the SV40 construct. (**A**) Schematic representation of two possible scenarios of replication termination in the SV40 construct. The blue tract indicates the 5.26-kb Bam HI–Sac I restriction fragment containing the SV40 origin, and the yellow tract indicates the 3.71-kb Sac I–Bam HI fragment, opposite to the origin. The red tract indicates the telomeric repeats. Normally, the two replication forks travel at similar distances to merge in the yellow region (pCtrl). If the clockwise fork stalls in the telomeric repeats, termination might occur also in the blue tract (pTelN). (**B**) 2D-gel analysis showing that the bulk of termination in the SV40 constructs (in both pCtrl and pTelN) occurs in the 3.71-kb Sac I–Bam HI fragment as expected [the yellow tract in the scheme in (A)]. DNA from the same experimental procedure, described in Fig. 1C, was separated in 2D-gels and hybridized with a ^{32}P-labeled Sac I–Bam HI 3.71-kb fragment from the pML113 construct. (**C**) Example of a double Y-shaped termination intermediate, visualized in the 5.26-kb fragment, containing the replication origin and the telomeric repeats from the pTelN construct. A scheme of the molecule visualized is shown above the image. The inset represents a magnification of the area inside the red square. Scale bar, 180 nm (0.5 kb). (**D**) Quantification of the fraction of termination intermediates visualized in the 5.26-kb Bam HI–Sac I fragment, from the three independent experiments described in Fig. 2B. Bars represent mean with SD. The *P* value was derived from unpaired, two-tailed Student's *t* test.

molecules were enriched by separating them from the linear form on a preparative agarose gel (fig. S2A) and only molecules with a size compatible with the Bam HI–Sac I restriction fragment (>60% of the replication intermediates isolated from the gel) were analyzed (fig. S2B). Normal forks were visualized either within a replication bubble or as three-way junctions. Events of replication fork reversal were visible either within a replication bubble or as X-shaped (four-way) DNA structures with two arms of equal length (Fig. 2A). Reversed forks were observed in both the pTelN, pTelR, and pCtrl fragment of matching length; however, the presence of telomeric repeats was associated with an over twofold increase in reversed replication forks (Fig. 2B). This result is consistent with the increase in cone signal intensity observed in 2D-gels and with previous EM analysis of model telomeric forks (*16*).

In the circular SV40 constructs, the two diverging forks originating from the SV40 origin typically travel a similar distance and converge on the opposite site of the origin (Fig. 3A). 2D-gel analysis of the other restriction fragment generated by the digestion—the 3.71-kb Sac I–Bam HI fragment—showed a strong termination signal, in both the control and pTelN construct (Fig. 3B). As expected, in EM analysis, the 5.26-kb fragment containing the SV40 origin showed very rare double Y-shaped termination intermediates; however, the presence of the telomeric repeats leads to a significant increase of termination intermediates detected in this fragment (Fig. 3, C and D). This result is consistent with an increased stalling frequency of the clockwise fork traveling through the telomeric repeats and consequent entry of the counterclockwise fork in the restriction fragment (Fig. 3A).

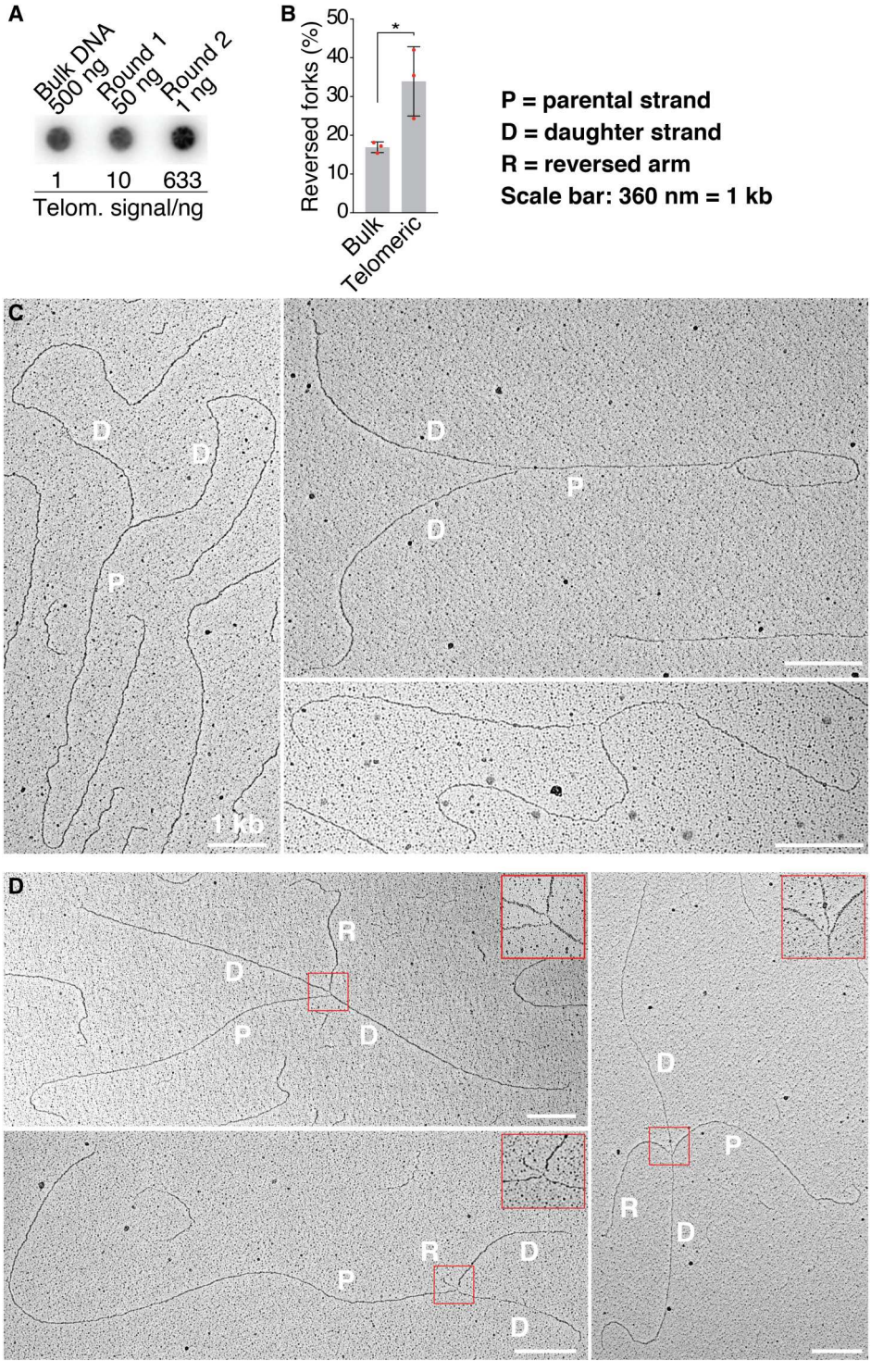

Fig. 4. Increased incidence of reversed forks at mouse telomeres. (**A**) Dot blot analysis showing the enrichment of telomeric repeats. Telomeres were enriched through two restriction digestion and size exclusion steps as described in (*31*). After each enrichment step, the amounts of DNA indicated in the figure were spotted on a membrane and hybridized with a ^{32}P-labeled probe recognizing telomeric repeats. The amount of TTAGGG repeat signal per nanogram was quantified and reported relative to the signal per nanogram value in the initial, nonenriched, bulk DNA. (**B**) Quantification of the percentage of molecules compatible with a reversed fork structure, over all replication forks from three independent experiments, where either telomere-enriched or Kpn I–digested bulk DNA was spread and visualized by EM. (A) $N = 81$, 74, and 144 and 64, 72, and 130 replication forks for telomeric and bulk samples, respectively. Bars represent mean with SD. The P value was derived from unpaired, two-tailed Student's t test. (**C**) Examples of normal replication forks from a telomere-enriched sample. (**D**) Examples of molecules compatible with a reversed fork structure from a telomere-enriched sample. Insets represent magnifications of the area inside the red square. Scale bars, 360 nm (1 kb).

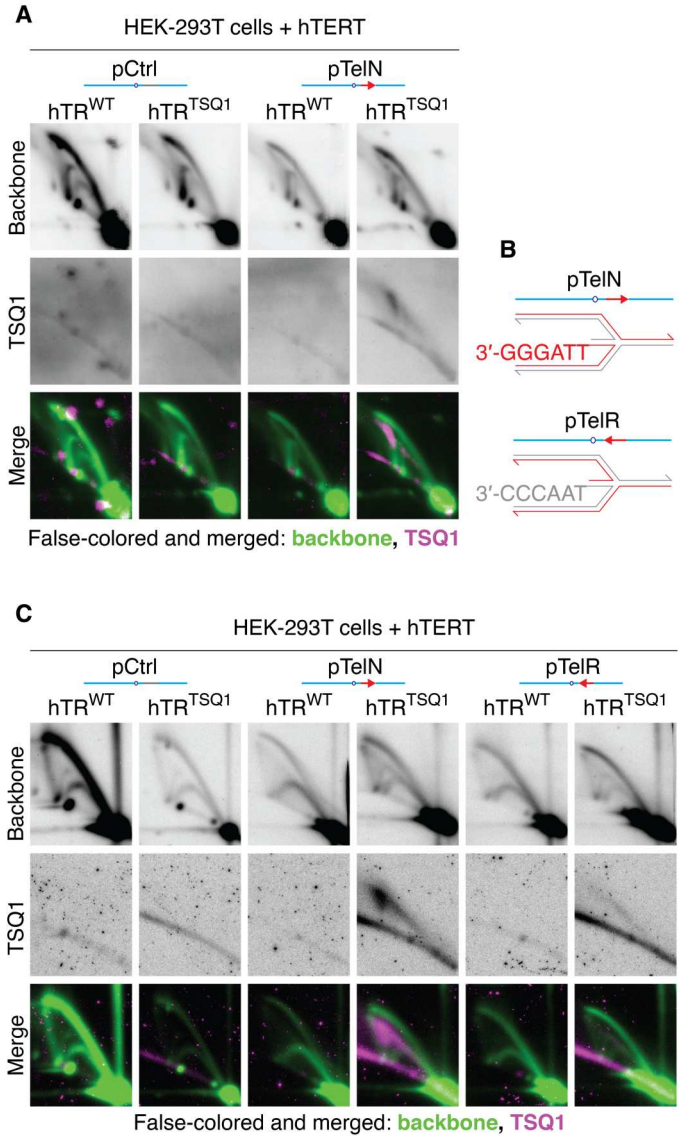

Fig. 5. Extension of reversed telomeric forks by telomerase. (**A**) 2D-gel experiments showing detection of the telomerase-dependent addition of TSQ1 repeats at the cone signal, where reversed forks migrate in 2D-gels. HEK-293T cells were transfected with the indicated constructs, and 40 hours after transfection, cells were collected and psoralen–cross-linked in vivo. Extra-chromosomal DNA was extracted with the Hirt procedure; digested with Bam HI, Sac I, and Dpn I; and separated in 2D-gels. The gels were blotted onto a membrane and hybridized with a ^{32}P-labeled (GCAACC)4 (TSQ1) oligo to detect telomerase extension events. Then, the membrane was stripped and hybridized with a ^{32}P-labeled Bam HI–Sac I 4.53-kb fragment from the pML113 construct (Backbone). To facilitate visualization, the images were false-colored and merged (bottom). (**B**) Schematic representation showing that the sequence of the 3′-end of the reversed arm will depend on the orientation of the telomeric repeats with respect to the clockwise moving fork. (**C**) 2D-gels showing that the telomerase-mediated extension of reversed forks depends on the orientation of the telomeric repeats. The same experimental procedure as the one described in (A) was performed, including the construct pTelR with the inverted orientation.

Increased incidence of replication fork reversal at mouse telomeres

Prompted by the results obtained at the ectopic telomeric repeats in the SV40 system, we asked if the increased frequency of replication fork reversal is observed also at endogenous telomeres. To address this point, we decided to analyze mouse telomeres by EM. Because this type of analysis is limited by the paucity of replication intermediates in the final sample, we exploited a rapidly dividing mouse B cell lymphoma line established from the lambda-*MYC* transgenic model with long telomeres (*30*). Telomeres from this cell line were enriched through two successive rounds of restriction digestion with frequent cutters, followed by size fractionation (Fig. 4A) (*31*). For EM analysis, Y-shaped molecules (replication forks) and X-shaped intermediates with two equal arms (compatible with fork reversal) were quantified in parallel in the nonenriched (bulk) DNA and after telomere enrichment (telomeric) (Fig. 4, B to D). In these experiments, telomere-enriched samples showed a twofold increase in the fraction of reversed forks, compared to the respective bulk DNA (Fig. 4B). These results were observed in the absence of any exogenously induced replication stress and show that, consistently with the replication of ectopic telomeric repeats, replication of endogenous telomeres is also associated with an increased probability of replication fork reversal.

Extension of reversed telomeric forks by the TERT in vivo

Several studies have suggested that reversed telomeric forks could become a substrate for the TERT (*19*–*21*). However, direct evidence for this activity is missing, also due to the inability to differentiate it from postreplicative elongation of telomeric double-strand breaks. We sought to take advantage of the SV40 mini-chromosome, bearing a long stretch of telomeric repeats, to address this question directly. This system offers two main advantages: First, it does not contain a natural telomeric end that would provide a substrate for telomerase, and second, its replication intermediates are readily visualized in 2D-gels, which could allow detection of telomerase activity on specific telomeric structures (see below). To label specifically telomerase extension events, we took advantage of a mutated version of the telomerase TR, *hTR-TSQ1* (tolerated sequence 1), which introduces a GTTGCG motif at telomeres (*22*). As expected, ectopic expression of the TERT (hTERT) together with a mutated *hTR-TSQ1* template in 293T cells leads to the addition of the GTTGCG motif at telomeres, detected by peptide nucleic acid (PNA)–FISH and, in telomere blots, hybridized with a TSQ1-specific probe (fig. S3, A and B). We then monitored, under the same conditions, telomerase activity at the telomeric replication intermediates in the SV40 mini-chromosome. The pCtrl or pTelN constructs were transfected together with *hTERT* and *hTR-TSQ1* and allowed to replicate, and then the 5.26-kb Bam HI–Sac I fragment was separated in 2D-gels as described above. The membranes were hybridized sequentially, first with a probe recognizing the TSQ1 repeats and then with another against the entire Bam HI–Sac I fragment (backbone). No TSQ1 signal was detected in the *hTR-WT* controls, or when *hTR-TSQ1* was expressed in cells replicating the pCtrl construct (Fig. 5A). However, when *hTR-TSQ1* was expressed in cells replicating the pTelN construct, a clear TSQ1 signal was visible in 2D-gels and the TSQ1 signal (deriving from telomerase activity) overlapped in 2D-gels with the cone signal that is generated by telomeric reversed forks (Fig. 5A and fig. S4A). Consistent with this observation, pTelN constructs with 34 or

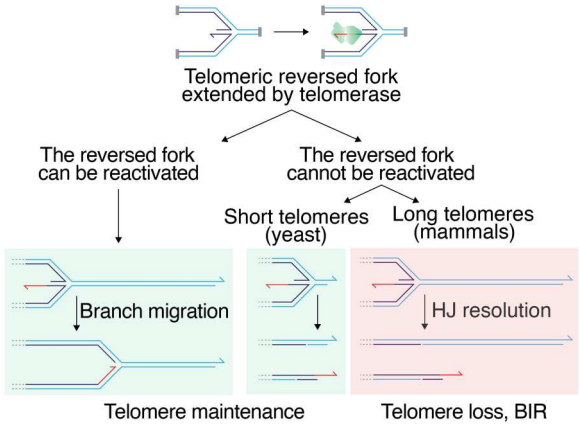

Fig. 6. Possible consequences of telomerase engagement at reversed forks. If reversed forks elongated by telomerase can be reactivated in a timely fashion, then telomere replication can be completed. In this scenario, telomerase elongation of the 3′-end may even assist the bypass of certain lesions on the leading strand. If reversed forks elongated by telomerase cannot restart, then telomeric repeats ahead of the fork cannot be copied by semiconservative DNA replication. In cells where the size of telomerase-extension events is comparable to the average telomere length (i.e., yeast), incomplete replication can be compensated for by telomerase. However, in cells with kilobase-long telomeres (i.e., mouse or human), this process would lead to the loss of the telomeric tract ahead of the reversed fork, which could then only be recovered by recombination-mediated mechanisms like BIR.

54 telomeric repeats (that have lower levels of fork reversal) showed the same pattern, but a fainter TSQ1 probe signal (fig. S4B). This result shows that telomerase can extend reversed telomeric forks in vivo.

We considered the possibilities that the TSQ1 sequence at the cone signal might derive from extension of telomeric double strand breaks (DSBs), which are then engaged in homologous recombination, and/or that recruitment of telomerase on ectopic telomeric repeats might lead to unspecific or spurious activities on telomeric reversed forks. To address these points, we repeated the experiment including a pTelR construct, which is identical to pTelN, except that the orientation of the telomeric repeats, with respect to the SV40 origin, is reversed. While this construct should be identical to pTelN in terms of telomerase recruitment and eventual extension of DSBs formed during the replication of telomeric repeats, reversal of the clockwise fork in the pTelR construct will generate a C-rich 3′-end that should not be targeted by telomerase (Fig. 5B). While a strong cone signal was detected by the TSQ1 probe in the pTelN construct, no cone signal was detected by the TSQ1 probe in the pTelR construct (Fig. 5C and fig. S4C). Therefore, the results obtained in 2D-gels cannot be attributed to an unspecific activity of the telomerase recruited at the ectopic telomeric repeats or extension of telomeric DSBs, but rather represent a bona fide telomerase activity extending reversed telomeric forks.

DISCUSSION

Fork reversal is thought to occur when the replication machinery encounters a roadblock on the template. This phenomenon is typically observed genome-wide after treatment with genotoxic agents that induce DNA strand damage, cross-links, inhibit replicative polymerases, or deplete the deoxynucleoside triphosphate (dNTP) pool (*32*). Tightly bound proteins and replication-transcription collisions have also been invoked as potential sources of fork reversal, while accumulation of positive supercoiling ahead of the fork has been shown to drive fork regression in reconstituted systems (*33*, *34*). We observe a nearly twofold increase in the incidence of reversed forks at telomeric repeats compared to a nontelomeric sequence in the SV40 system or to the bulk genomic DNA in mouse cells. While the absolute levels of fork reversal that we observe may be influenced by the experimental tools used here, such as the deregulated expression of the MYC oncogene in the mouse B cell lymphoma line, or the use of the large T-antigen helicase in the SV40 constructs, comparison with the nontelomeric, control DNA replicated exactly under the same conditions indicates that mammalian telomeric repeats are hotspots for replication fork reversal. Our results are consistent with long-standing observations of telomeres being hard-to-replicate regions from yeast to mammals (*4*, *8*, *17*, *18*). Reversed forks at ectopic telomeric repeats in the SV40 system occurred in an orientation-independent manner and were not affected by treatment with the G4-stabilizing ligand pyridostatin. These results argue against G4-DNA being a major driver of fork reversal at telomeric repeats, at least in the episomal, SV40 setting. The experiments with ectopic repeats also indicate that reversed forks can occur in the absence of a t-loop structure. Other potential obstacles to telomere replication include the presence of damage-induced i-loops, or tightly bound shelterin subcomplexes that need to be removed at the passage of the replication fork (*12*–*15*, *18*). Other intrinsic features of stretches of repetitive DNA, like the abundance of local homology, could also contribute to replication fork reversal at telomeres (*16*, *23*). Formation of reversed forks during telomere replication could have important consequences for telomere metabolism. The observation that the SMARCAL1 helicase, which is thought to promote fork reversal, is also required for telomere integrity suggests that fork reversal might be a mechanism that deals with replication stress at telomeres (*35*, *36*). The reversed arm would generate an unprotected end, which could, in principle, lead to the activation of a double-strand break response at telomeres (*37*). Furthermore, the reversed arm could be engaged in interchromosomal break-induced replication (BIR), favored by the abundance of homology at telomeric repeats. This would be consistent with reports of BIR in conditions associated with telomere replication stress (*38*–*40*).

Our 2D-gel experiments reveal telomerase-mediated extension events on DNA structures migrating in the cone signal. This observation implies generation of the reversed arm in vivo, providing orthogonal evidence to the visualization of reversed forks in EM. Furthermore, they imply that telomerase can be recruited at a reversed telomeric fork, where it can add telomeric repeats, extending the reversed arm. The consequences of this process on telomere maintenance will depend on at least two factors: (i) the ability of telomeric reversed forks to restart and (ii) the length of the unreplicated telomeric repeats ahead of the reversed fork. If a telomeric reversed fork is unable to restart, the telomeric tract downstream the fork cannot be completed by semiconservative replication. If this tract exceeds the repeats that telomerase can add in one S phase, then this process will result in the loss of telomeric repeats (Fig. 6). This scenario would apply to mammalian cells with long telomeres and is consistent with the phenotype of RTEL1-deleted mouse cells, characterized by telomerase-dependent telomere loss.

In that setting, it was suggested that abnormal telomerase loading at telomeres prevented the restart of telomeric reversed forks (*21*). However, if telomerase activity can fully compensate for the length of telomeric repeats ahead of the reversed forks, then the process will not result in the loss of telomeric repeats, but rather it might have the advantage of elongating telomeres during replication, without generating two newly replicated and unprotected sister ends that would be at risk of fusion (Fig. 6). This scenario is consistent with the proposed mechanisms of telomere elongation in yeast, where telomerase extension events are comparable to the average telomere length (*19*, *20*, *41*). A similar scenario could be envisioned also for mammalian cells, with long telomeres, if telomerase recruitment and/or fork reversal occurs near the 3′-end of the chromosome, similarly to what have been proposed for replication forks encountering a DSB (*42*). Last, unscheduled telomerase activity at reversed forks might contribute to the instability of interstitial telomeric repeats, especially in telomerase-positive cells experiencing replication stress, a recurrent condition in cancer cells.

MATERIALS AND METHODS

Plasmids and cloning

All the SV40 constructs derive from pML113 (*23*). A Bsm BI site, leaving Eco RI compatible ends, was introduced next to the Kpn I site of pML113 to generate pSV40. For the constructs with 34 telomeric repeats, an insert containing 34 TTAGGG repeats was amplified by polymerase chain reaction (PCR) from pTH5, a gift from T. de Lange, with the following oligos: forward: 5′-TACGGGTACCAATTCGGCCTAATTCGGCCT; reverse: 5′-TCAGGGTACCAATTCGGCCAAATTCGGTAG. The PCR product was digested with Kpn I and introduced into Kpn I–linearized pML113. To generate the constructs with 54 and 115 repeats, an Eco RI fragment containing TTAGGG repeats from pTH9 (a gift from T. de Lange) was introduced into Bsm BI–linearized pSV40, and products with one or two insertions in tandem, in either orientation, were selected. For matching size controls (pCtrl), fragments of 200, 400, and 800 base pairs (bp) (for inserts with 34, 54, and 115 telomeric repeats, respectively) were amplified from the hygromycin resistance marker of pHEBO (a gift from T. de Lange) (*43*) with Eco RI–compatible ends and were introduced into Bsm BI–digested pSV40. For *hTERT* and *hTR-TSQ1* expression, cells were transfected with pcDNA-3F-hTERT-WT, pBlueScript-U1-hTR-WT, or pBlueScript-U1-hTR-TSQ1.

Cell culture

HEK-293T Interlab Cell Line Collection (ICLC) cells were grown in Dulbecco′s modified Eagle′s medium (DMEM) (Lonza, BE12-614F), supplemented with 10% fetal bovine serum (EuroClone, ECS0180L) and 2 mM L-glutamine (EuroClone, LOBE17605F). The mouse B cell lymphoma line #126800 was established from a lambda-MYC transgenic animal, and early-passage cells were maintained in DMEM (Lonza, BE12-614F), supplemented with 10% fetal bovine serum (EuroClone, ECS0180L), 2 mM L-glutamine (EuroClone, LOBE17605F), 0.1 mM nonessential amino acids (Microtech, X-0557), 1 mM sodium pyruvate (Microtech, L0642), and 40 μM 2-mercaptoethanol (Life Technologies, 31350-010). Cells were diluted to 1×10^5 cells/ml in new plate every 2 days. Transfection of HEK-293T cells was performed with the calcium phosphate method. Cells (6×10^6 to 7×10^6) were plated in a 15-cm dish (~50% confluency) 1 day before the transfection. For each plate, 190 μl of $CaCl_2$ (2 M) together with 15 μg of plasmid DNA and 1 μg of pAcGFP1-C1 (Clontech, 632470), in 1500-μl final volume of ddH_2O, were mixed with an equal amount of HEPES-buffered saline (HBS) (2×). During the process of mixing, the solution was aerated by blowing air through a 2-ml pipette with Pipet-Aid; then, the solution was added dropwise to the cells. The medium was changed 16 to 18 hours after transfection. Alternative cells were transfected with polyethylenimine (PEI Max 40,000, PEI 2500, Histo-Line Laboratories, catalog no. 24765-1). Cells were transfected at 50 to 70% confluence. The medium was changed 30 min before transfection. For each 15-cm plate containing 20 ml of medium, the DNA (10 to 15 μg per construct) is diluted in DMEM to a final volume of 150 μl. PEI (stock 1 mg/ml) is diluted 1:10 to a final volume of 150 μl for each 15-cm plate. The PEI and DNA dilutions were mixed 1:1, vortexed briefly, and incubated for 10 min at room temperature (RT). The mix was added dropwise to the cells and gently distributed by rocking the plate back and forth. The medium was changed again 1 day after the transfection. When indicated, cells were treated with 50 μM pyridostatin (Sigma-Aldrich, SML0678) 1 hour before the harvest. Psoralen cross-linking was performed as described in (*31*). Briefly, cells resuspended in 3 ml of ice-cold Dulbecco's phosphate-buffered saline (DPBS) with Ca^{++} and Mg^{++} (Life Technologies, 14080-089) were poured in a 6-cm dish and kept on ice, in the dark, while stirring, throughout the procedure. The suspension was first incubated with 4,5′,8-trimethylpsoralen (~7 μg/ml) (Sigma-Aldrich, T6137; stock 2 mg/ml in dimethyl sulfoxide, stored at −20°C) for 5 min in the dark and then exposed to 365-nm ultraviolet (UV) light for 2.5 min in UV Stratalinker 1800 (Stratagene), with 365-nm UV bulbs (model UVL-56, UVP) at 2 to 3 cm from the light source.

Hirt extraction of extrachromosomal DNA (ecDNA)

The plasmid DNA was recovered using a modified Hirt protocol (*24*, *44*). Cells were washed with 4 ml of ice-cold tris-buffered saline [50 mM tris-HCl (pH 7.0) and 150 mM NaCl] and lysed by incubation for 20 min at RT in 0.7 ml of lysis solution [50 mM tris-HCl (pH 7.0), 20 mM EDTA, 10 mM NaCl, 2% SDS, and proteinase K (0.4 mg/ml)]. Then, chromosomal DNA was precipitated by the addition of 0.3 ml of 5 M NaCl, followed by overnight incubation at 4°C. The samples were centrifuged in a SW41-Ti rotor (Beckman) at 16,000 rpm (31,611*g*) for 50 min at 4°C, and the supernatant (~1 ml) was collected, supplemented with 2 μl of proteinase K (Roche, 31158870015, stock 50 mg/ml), and incubated at 55°C for 2 hours. DNA was extracted with 1 volume of phenol/chloroform/isoamyl alcohol (25:24:1; Sigma-Aldrich, P2069) and chloroform extraction, followed by precipitation with isopropanol.

Two-dimensional agarose gel electrophoresis

Around 3 to 4 μg of plasmid DNA, extracted from 293T cells with the procedure described above, were digested as follows: The plasmids with 115 repeats were digested overnight with 90 U of Sac I and Bam HI. The day after, 40 U of Dpn I (NEB) was added and the digestion was incubated again at 37°C for 1 hour. The plasmids with 34 and 54 telomeric repeats were digested with 90 U of Eco RI and Not I, respectively, overnight at 37°C and 1 additional hour with 40 U of Dpn I. The digestion was precipitated with isopropanol and resuspended in 10 mM tris-HCl (pH 8.0). The first

dimension was run on 0.4% agarose (US Biological, A1015) in 0.5× tris-borate-EDTA (TBE) without ethidium bromide (EtBr) for 42 hours at 0.65 V/cm. Subsequently, the first dimension was stained in 0.5× TBE with EtBr for 45 min. For each lane, a slice of 6.5 cm from the 5-kb size and up was cleaved. The second dimension was run on 0.7% agarose gel with EtBr for 23 hours at 2 to 3 V/cm at 4°C. Before blotting, psoralen cross-linking was reversed by irradiating the gel for 10 min under 254-nm UV light (UVP CL1000 Ultraviolet crosslinker). For Southern blotting, the gel was first incubated for 30 min with the depurination solution (0.25 N HCl), 2 × 40 min with denaturing solution (0.5 M NaOH and 1.5 M NaCl), and 2 × 40 min with neutralizing solution [0.5 M tris (pH 7.5) and 3 M NaCl]. The DNA was then transferred by capillarity in 10× SSC onto an Amersham Hybond-X membrane (GE Healthcare, RPN203). Probes were labeled with the Prime-a-Gene Labeling system (Promega, U1100) using [α-^{32}P]deoxycytidine triphosphate (dCTP) (3000 Ci/μmol; PerkinElmer, 1300000327). For the TSQ1 repeat detection, the oligonucleotides (complementary of TSQ1 sequence or forward TSQ1 sequence) were end-labeled with T4-PNK (NEB, M0201) and [γ-^{32}P]adenosine triphosphate (ATP) (6000 Ci/μmol; PerkinElmer, 1300000372).

Alternatively, the TSQ1-hi-a (5′-AAACCGCAACCGCAACCG-CAACCGC) and Template-TSQ1-hi-a (3′-TTTGGCGUUGGC-GUUGGCGUUGGCG) oligos were used to generate a probe as described in (*45*). Briefly, the oligos were annealed by mixing 3.4 μl of 10 μM Template-TSQ1-hi-a and 15.6 μl of 100 μM TSQ1-high activity with 1 μl of 1 M NaCl and incubating at 99°C for 1 min, 37°C for 15 min, then at RT for 15 min. The labeling reaction was set up mixing pre-annealed template oligos with 50 μM deoxyadenosine triphosphate (dATP) and deoxyguanosine triphosphate (dGTP) (Invitrogen, catalog no. 15612-01), 5 μl of [α-^{32}P]dCTP, and 5 U of DNA polymerase I Klenow fragment (Promega, catalog no. M220A) in a final volume of 25 μl in buffer M [10 mM tris (pH 7.6), 10 mM $MgCl_2$, 50 mM NaCl, 0.5 mM dithiothreitol (DTT), and bovine serum albumin (400 ng/μl)]. The reaction was incubated for 20 min at RT and then at 95°C for 5 min. After cooling down to RT, 5 U of uracil deglycosylase (NEB, BM0280S) was added and the reaction was incubated at 37°C for 10 min and then at 98°C for 10 min. The volume was brought to 50 μl with TES (tris-EDTA-SDS), passed through a microspin G25 column (GE Healthcare, GE275325), and diluted in the hybridization mix (Church mix). Hybridization was carried out overnight at 50°C. The membranes were washed three times with 4× SSC for 30 min each and with 4× SSC, 0.1% SDS for another 30 min at 50°C. For the detection of telomeres, the pSty11 plasmid was digested with Eco RI, and the 800-bp fragment was purified from the gel and diluted at 20 ng/μl in ddH_2O. Ten microliters (200 ng) of the 800-bp telomeric insert was mixed with 5 μl of telomeric oligo (1 ng/μl) and 24 μl of ddH_2O, incubated at 95°C for 5 min, and quickly chilled on ice. For probe labeling, 5 μl of the 10× reaction buffer, 5 μl of [α-^{32}P]dCTP (3000 Ci/μmol; PerkinElmer, 1300000370), and 5 U of DNA polymerase I Klenow fragment were added, incubated at RT for 90 min. The probe was passed through a microspin G50 column (GE Healthcare, GE27533001), incubated at 95°C for 5 min, and chilled on ice before being diluted in the hybridization mix. Hybridization was carried out at 65°C for at least 4 hours to overnight. The membrane was washed twice for 15 min with 2× SSC at 65°C and exposed on a phosphoscreen for 2 hours. Radioactive signal was captured on phosphor screens (FUJIFILM Storage Phosphor screen MS3543 E), read on Typhoon Trio (GE), and analyzed on ImageJ.

Quantitative PCR

Two 10-cm plates of HEK-293T were transfected with a 1:1 mix of pTelN and pCtrl. Forty hours after transfection, plasmid DNA was extracted using the Hirt protocol. Quantitative PCR (qPCR) was performed using LightCycler 480 (Roche), and the amplifications were done using SsoFast EvaGreen Supermix (Bio-Rad, 1725201), according to the manufacturer's indications. The following primers recognizing the SV40 backbone were used as an internal control: SV40_qPCR_Fw: 5′-GATAATGCTTATCCAGTGGA; SV40_qPCR_Rev: 5′-GTAGGTTCCAAAATATCTAG. The primer couple for the pTelN plasmid was as follows: SV40_Fw: 5′-CCCTAACCCTCCGAATTGGA; Telo-specific_Rev: 5′-CCCTAACTGACACACATTCC. The primer couple for the pCtrl plasmid was as follows: SV40_Fw: 5′-CCCTAACTGACACA-CATTCC; Random-specific_Rev: 5′-GTCAGGCTCTCGCAATTG-GA. Reactions were carried out in triplicate for each set of data. The relative quantification in plasmid replication was determined using the $2^{-\Delta\Delta Ct}$ method (*46*), obtaining the fold changes in plasmid replication, normalized with the Ct of the internal control.

Chromatin immunoprecipitation

Four- to 15-cm plates for each condition, containing 20 ml of medium each, were cross-linked for 10 min at RT by adding 540 μl of 37% formaldehyde (Merck, 104002) and incubating with gentle shaking. Formaldehyde was quenched for 5 min with 125 mM glycine. Cells were scraped with 1× PBS, keeping the plates on ice. Chromatin extraction was prepared by lysing in four different buffers: Buffer A [100 mM tris-HCl (pH 8.0) and 10 mM DTT] for 15 min at RT and 15 min at 30°C, Buffer B [10 mM Hepes (pH 7.5), 10 mM EDTA, 0.5 mM EGTA, and 0.25% Triton X-100] for 5 min on ice, Buffer C [10 mM Hepes (pH 7.5), 10 mM EDTA, 0.5 mM EGTA, and 200 mM NaCl] for 5 min on ice, and Buffer D [50 mM tris-HCl (pH 8.0), 10 mM EDTA, 1% SDS, and 1× proteinase inhibitor cocktail]. Then, the chromatin was sonicated for 10 cycles, 30 s on and 30 s off on Bioruptor Plus (Diagenode). The chromatin was resuspended in 10 volumes of dilution buffer [16.7 mM tris-HCl (pH 8.0), 167 mM NaCl, 1.2 mM EDTA, and 1.1% Triton X-100], on a concentration of 100 μg for each condition, and precleared with 100 μl of blocking beads, prepared for 2 hours at 4°C with 40 μl of Dynabeads Protein G beads (Thermo Fisher Scientific, 10003D), 10 μl of anti-TRF1 antibody (Santa Cruz, GO715), and IP dilution buffer [1.1% Triton X-100, 1.2 mM EDTA, 16.7 mM tris-HCl (pH8), and 150 mM NaCl]. After overnight incubation at 4°C, beads were washed three times for 5 min with a low-salt washing buffer [0.5% Triton X-100, 5 mM EDTA, 50 mM tris-HCl (pH 8.0), and 150 mM NaCl]. Beads were then resuspended in 500 μl of elution buffer (0.1 M $NaHCO_3$ and 1% SDS) for 40 min at RT and subsequently decross-linked by adding 36 μl tris-HCl 1M (pH 8.0), 182 mM NaCl, and proteinase K (360 μg/ml; Roche) and incubated for 2 hours at 52°C and then overnight at 65°C. The DNA was purified using the phenol/chloroform/isoamyl alcohol and eluted in 30 μl of 10 mM tris-HCl buffer. qPCR was performed with LightCycler 480 (Roche) combining 1 μl of DNA with 18 μl of SsoFast EvaGreen Supermix (Bio-Rad, 1725201) and the following primers: forward: 5′-

GGACTTTCCACACCTGGTTG; reverse: 5′-GGAGACGGGTACCTTCTGAG, according to the manufacturer′s indications.

Purification of SV40 replication intermediates for EM

Digested DNA was separated on a preparative gel [0.6% (w/v) low-melting agarose (Lonza, catalog no. 50100) gel in 1× tris-acetate-EDTA (TAE)]. The gel was run at 0.8 V/cm for 1 hour and at 2 V/cm for 2 hours. The lane portion above the 5.2-kb fragment was excised, and the DNA was recovered with the silica bead DNA gel extraction kit (Thermo Fisher Scientific, K0513) following the manufacturer′s instructions, except that, once the DNA was bound, the beads were not resuspended to avoid mechanical shearing of the DNA. The DNA was eluted in 1× TE and quantified using a Qubit dsDNA HS assay kit (Invitrogen, Q32854).

Enrichment of telomeric repeats

Cells (500×10^6) were used for the telomere enrichment procedure as described in detail in (*31*).

EM spreading, acquisition, and analysis

EM analysis was performed according to (*26*). Typically, 5 μl of telomere-enriched DNA corresponding to 20 to 100 ng was used for each spread. The DNA was added to premixed 5 μl of formamide (Thermo Fisher Scientific, 17899) and 0.4 μl of 0.02% benzalkonium chloride (BAC; Sigma-Aldrich, B6285) in TE (0.2% BAC stock solution in formamide was diluted 1:10 in 1× TE before use). After mixing, the drop was immediately spread on a water surface in a 15-cm dish containing 50 ml of distilled water, using a freshly cleaved mica sheet (Ted Pella Inc., product no. 52-6) as a ramp. For nonenriched controls, 30 ng of Kpn I–digested genomic DNA was spread using the same method. The monomolecular layer was gently touched with an EM grid prepared as follows. A thin (4 to 8 nm), homogeneous, and low-grain carbon layer was deposited on EM grids (Nanovision, PEG400). The carbon layer was created on a mica glass surface (2 cm × 2 cm) using the MED020 e-beam evaporator (Leica), equipped with the QSG monitor, two EK030 electron guns controlled by the EVM030 control unit. The e-beam evaporation parameters described in the instruction manual were used. The carbon layer deposited on the mica surface was floated on the surface of the water and transferred on the 400-mesh copper grids. Before use, carbon-coated EM grids were placed in contact with an ethidium bromide solution (33.3 μg/ml in H_2O) for 30 to 45 min at RT. Carbon grids with absorbed DNA molecules were immediately stained with a solution of uranyl acetate (0.2 μg/μl) in ethanol and coated with 8 nm of platinum using the MED020 evaporator modified with the low-angle grid shadowing kit (Leica 16770525) so that the sample holder was placed at an angle of 280.5° and made an angle of around 3° with the platinum gun fixed on the head of the instrument. For platinum e-beam evaporation, we used the parameters indicated in the MED020 instruction manual. TEM pictures were taken using a FEI Tecnai12 BioTwin microscope operated at 120 kV and equipped with a side-mounted GATAN Orius SC-1000 camera controlled by the Digital Micrograph software. Images in DM3 format were analyzed using the ImageJ software. In these conditions, 0.36 μm corresponds to 1 kb of double-stranded DNA. Molecules with reversed arm inside a replication bubble or X-shaped molecules with two equal arms were scored as reversed forks.

Telomere blots

Genomic DNA was extracted from 10^7 cells with phenol/chloroform/isoamyl alcohol, as described in (*31*). Thirty micrograms of genomic DNA was digested overnight with 150 U of Hin fI and Rsa I and separated on a 0.8% agarose gel in 1× TAE at 1.8 V/cm for 16 hours. The gel was blotted onto a membrane and hybridized with ^{32}P-labeled probes as described above.

Fluorescence in situ hybridization

HEK-293T cells were plated onto glass coverslips 2 days after the transfection. The next day, the cells were fixed with formaldehyde 4% for 10 min at RT and then washed with PBS. The cells were dehydrated in ethanol series 70%-90%-100%, 5 min each, and then air-dried. The coverslips were then incubated with the hybridizing solution [70% formamide, Thermo Fisher Scientific, 17899; 10 mM tris (pH 7.4), 0.5% blocking reagent, Roche, 11096176001] with a mix of Cy5-labeled (TTAGGG)3 probe (PNA Bio) and CY3-labeled (CGCAAC)3 PNA probe (Panagene) (1:500; stock 54 μM, used 100 nm each). The coverslips were incubated for 5 min at 80°C and then overnight at RT. The coverslips were washed twice with wash buffer I [70% formamide and 10 mM tris (pH 7.4)] at RT, once with PBS-Tween (0.1% final) with 4′,6-diamidino-2-phenylindole (DAPI) (0.5 mg/ml, 3000×), and once with PBS-Tween, dehydrated in ethanol series 70%-90%-100%, 5 min each, air-dried, and mounted with ProLong Gold antifade reagent (Invitrogen, catalog no. P36930). The images were acquired on a DV Elite system (GE Healthcare) equipped with an IX71 microscope (Olympus) and a scientific complementary metal-oxide semiconductor (sCMOS) camera and driven by SoftWoRx version 7.0.0 and analyzed in ImageJ.

Supplementary Materials

This PDF file includes:

Figs. S1 to S4

REFERENCES AND NOTES

1. T. de Lange, Shelterin-mediated telomere protection. *Annu. Rev. Genet.* **52**, 223–247 (2018).
2. R. A. Wu, H. E. Upton, J. M. Vogan, K. Collins, Telomerase mechanism of telomere synthesis. *Annu. Rev. Biochem.* **86**, 439–460 (2017).
3. L. Crabbe, R. E. Verdun, C. I. Haggblom, J. Karlseder, Defective telomere lagging strand synthesis in cells lacking WRN helicase activity. *Science* **306**, 1951–1953 (2004).
4. A. Sfeir, S. T. Kosiyatrakul, D. Hockemeyer, S. L. MacRae, J. Karlseder, C. L. Schildkraut, T. de Lange, Mammalian telomeres resemble fragile sites and require TRF1 for efficient replication. *Cell* **138**, 90–103 (2009).
5. P. Martinez, M. Thanasoula, P. Muñoz, C. Liao, A. Tejera, C. M. Nees, J. M. Flores, O. Fernández-Capetillo, M. Tarsounas, M. A. Blasco, Increased telomere fragility and fusions resulting from TRF1 deficiency lead to degenerative pathologies and increased cancer in mice. *Genes Dev.* **23**, 2060–2075 (2009).
6. J.-B. Vannier, V. Pavicic-Kaltenbrunner, M. I. Petalcorin, H. Ding, S. J. Boulton, RTEL1 dismantles T loops and counteracts telomeric G4-DNA to maintain telomere integrity. *Cell* **149**, 795–806 (2012).
7. M. Zimmermann, T. Kibe, S. Kabir, T. de Lange, TRF1 negotiates TTAGGG repeat-associated replication problems by recruiting the BLM helicase and the TPP1/POT1 repressor of ATR signaling. *Genes Dev.* **28**, 2477–2491 (2014).
8. K. M. Miller, O. Rog, J. P. Cooper, Semi-conservative DNA replication through telomeres requires Taz1. *Nature* **440**, 824–828 (2006).
9. G. Sarek, J.-B. Vannier, S. Panier, J. H. J. Petrini, S. J. Boulton, TRF2 recruits RTEL1 to telomeres in S phase to promote t-loop unwinding. *Mol. Cell* **57**, 622–635 (2015).
10. E. Gilson, V. Géli, How telomeres are replicated. *Nat. Rev. Mol. Cell Biol.* **8**, 825–838 (2007).

11. B. Silva, R. Arora, S. Bione, C. M. Azzalin, TERRA transcription destabilizes telomere integrity to initiate break-induced replication in human ALT cells. *Nat. Commun.* **12**, 3760 (2021).
12. G. Mazzucco, A. Huda, M. Galli, D. Piccini, M. Giannattasio, F. Pessina, Y. Doksani, Telomere damage induces internal loops that generate telomeric circles. *Nat. Commun.* **11**, 5297 (2020).
13. R. Ohki, F. Ishikawa, Telomere-bound TRF1 and TRF2 stall the replication fork at telomeric repeats. *Nucleic Acids Res.* **32**, 1627–1637 (2004).
14. M. E. Douglas, J. F. X. Diffley, Budding yeast Rap1, but not telomeric DNA, is inhibitory for multiple stages of DNA replication in vitro. *Nucleic Acids Res.* **49**, 5671–5683 (2021).
15. E. A. Radchenko, A. Y. Aksenova, K. V. Volkov, A. A. Shishkin, Y. I. Pavlov, S. M. Mirkin, Partners in crime: Tbf1 and Vid22 promote expansions of long human telomeric repeats at an interstitial chromosome position in yeast. *PNAS Nexus* **1**, pgac080 (2022).
16. N. Fouché, S. Ozgür, D. Roy, J. D. Griffith, Replication fork regression in repetitive DNAs. *Nucleic Acids Res.* **34**, 6044–6050 (2006).
17. S. Makovets, I. Herskowitz, E. H. Blackburn, Anatomy and dynamics of DNA replication fork movement in yeast telomeric regions. *Mol. Cell. Biol.* **24**, 4019–4031 (2004).
18. A. S. Ivessa, J. Q. Zhou, V. P. Schulz, E. K. Monson, V. A. Zakian, Saccharomyces Rrm3p, a 5′ to 3′ DNA helicase that promotes replication fork progression through telomeric and subtelomeric DNA. *Genes Dev.* **16**, 1383–1396 (2002).
19. S. Matmati, S. Lambert, V. Géli, S. Coulon, Telomerase repairs collapsed replication forks at telomeres. *Cell Rep.* **30**, 3312–3322.e3 (2020).
20. P.-M. Dehe, O. Rog, M. G. Ferreira, J. Greenwood, J. P. Cooper, Taz1 enforces cell-cycle regulation of telomere synthesis. *Mol. Cell* **46**, 797–808 (2012).
21. P. Margalef, P. Kotsantis, V. Borel, R. Bellelli, S. Panier, S. J. Boulton, Stabilization of reversed replication forks by telomerase drives telomere catastrophe. *Cell* **172**, 439–453.e14 (2018).
22. M. E. Diolaiti, B. A. Cimini, R. Kageyama, F. A. Charles, B. A. Stohr, In situ visualization of telomere elongation patterns in human cells. *Nucleic Acids Res.* **41**, e176 (2013).
23. C. Follonier, J. Oehler, R. Herrador, M. Lopes, Friedreich's ataxia-associated GAA repeats induce replication-fork reversal and unusual molecular junctions. *Nat. Struct. Mol. Biol.* **20**, 486–494 (2013).
24. B. Hirt, Selective extraction of polyoma DNA from infected mouse cell cultures. *J. Mol. Biol.* **26**, 365–369 (1967).
25. Z. Deng, C. Atanasiu, J. S. Burg, D. Broccoli, P. M. Lieberman, Telomere repeat binding factors TRF1, TRF2, and hRAP1 modulate replication of Epstein-Barr virus OriP. *J. Virol.* **77**, 11992–12001 (2003).
26. M. Lopes, Electron microscopy methods for studying in vivo DNA replication intermediates. *Methods Mol. Biol.* **521**, 605–631 (2009).
27. M. Lopes, C. Cotta-Ramusino, A. Pellicioli, G. Liberi, P. Plevani, M. Muzi-Falconi, C. S. Newlon, M. Foiani, The DNA replication checkpoint response stabilizes stalled replication forks. *Nature* **412**, 557–561 (2001).
28. J. Courcelle, J. R. Donaldson, K. H. Chow, C. T. Courcelle, DNA damage-induced replication fork regression and processing in *Escherichia coli*. *Science* **299**, 1064–1067 (2003).
29. D. T. Long, K. N. Kreuzer, Regression supports two mechanisms of fork processing in phage T4. *Proc. Natl. Acad. Sci. U.S.A.* **105**, 6852–6857 (2008).
30. A. L. Kovalchuk, C.-F. Qi, T. A. Torrey, L. Taddesse-Heath, L. Feigenbaum, S. S. Park, A. Gerbitz, G. Klobeck, K. Hoertnagel, A. Polack, G. W. Bornkamm, S. Janz, H. C. Morse III, Burkitt lymphoma in the mouse. *J. Exp. Med.* **192**, 1183–1190 (2000).
31. G. Mazzucco, A. Huda, M. Galli, E. Zanella, Y. Doksani, Purification of mammalian telomeric DNA for single-molecule analysis. *Nat. Protoc.* **17**, 1444–1467 (2022).
32. K. J. Neelsen, M. Lopes, Replication fork reversal in eukaryotes: From dead end to dynamic response. *Nat. Rev. Mol. Cell Biol.* **16**, 207–220 (2015).
33. J. Atkinson, P. McGlynn, Replication fork reversal and the maintenance of genome stability. *Nucleic Acids Res.* **37**, 3475–3492 (2009).
34. L. Postow, C. Ullsperger, R. W. Keller, C. Bustamante, A. V. Vologodskii, N. R. Cozzarelli, Positive torsional strain causes the formation of a four-way junction at replication forks. *J. Biol. Chem.* **276**, 2790–2796 (2001).
35. L. A. Poole, R. Zhao, G. G. Glick, C. A. Lovejoy, C. M. Eischen, D. Cortez, SMARCAL1 maintains telomere integrity during DNA replication. *Proc. Natl. Acad. Sci. U.S.A.* **112**, 14864–14869 (2015).
36. K. P. Bhat, D. Cortez, RPA and RAD51: Fork reversal, fork protection, and genome stability. *Nat. Struct. Mol. Biol.* **25**, 446–453 (2018).
37. R. E. Verdun, L. Crabbe, C. Haggblom, J. Karlseder, Functional human telomeres are recognized as DNA damage in G2 of the cell cycle. *Mol. Cell* **20**, 551–561 (2005).
38. R. L. Dilley, P. Verma, N. W. Cho, H. D. Winters, A. R. Wondisford, R. A. Greenberg, Break-induced telomere synthesis underlies alternative telomere maintenance. *Nature* **539**, 54–58 (2016).
39. Z. Yang, K. K. Takai, C. A. Lovejoy, T. de Lange, Break-induced replication promotes fragile telomere formation. *Genes Dev.* **34**, 1392–1405 (2020).
40. R. M. Porreca, E. Herrera-Moyano, E. Skourti, P. P. Law, R. Gonzalez Franco, A. Montoya, P. Faull, H. Kramer, J.-B. Vannier, TRF1 averts chromatin remodelling, recombination and replication dependent-break induced replication at mouse telomeres. *eLife* **9**, e49817 (2020).
41. E. Bonnell, E. Pasquier, R. J. Wellinger, Telomere replication: Solving multiple end replication problems. *Front. Cell Dev. Biol.* **9**, 668171 (2021).
42. Y. Doksani, R. Bermejo, S. Fiorani, J. E. Haber, M. Foiani, Replicon dynamics, dormant origin firing, and terminal fork integrity after double-strand break formation. *Cell* **137**, 247–258 (2009).
43. J. L. Yates, N. Warren, B. Sugden, Stable replication of plasmids derived from Epstein-Barr virus in various mammalian cells. *Nature* **313**, 812–815 (1985).
44. G. S. Chandok, K. K. Kapoor, R. M. Brick, J. M. Sidorova, M. M. Krasilnikova, A distinct first replication cycle of DNA introduced in mammalian cells. *Nucleic Acids Res.* **39**, 2103–2115 (2011).
45. Y. Zhao, J. W. Shay, W. E. Wright, Telomere G-overhang length measurement method 1: The DSN method. *Methods Mol. Biol.* **735**, 47–54 (2011).
46. K. J. Livak, T. D. Schmittgen, Analysis of relative gene expression data using real-time quantitative PCR and the $2^{-\Delta\Delta CT}$ method. *Methods* **25**, 402–408 (2001).

Acknowledgments: We are grateful to the IFOM cell biology unit, IFOM imaging facility for support, and M. Giannattasio for assistance with EM. We thank M. Lopes for providing the pML113 plasmid and technical advice. We thank T. de Lange for providing the plasmids with telomeric repeats. We are grateful to F. Pessina for assistance with the ChIP and qPCR experiments and E. Zanella for critical reading. **Funding:** This work was supported by the Associazione Italiana per la Ricerca sul Cancro, AIRC, IG 19901 (to A.H., G.M., M.G., and Y.D.); Concern Foundation (to Y.D.); Associazione Italiana per la Ricerca sul Cancro, AIRC, IG 23747 (to S.C.); Umberto Veronesi Foundation (to V.P.); National Cancer Institute (NCI) grant P30CA006927 (to L.C.); and National Institute of Allergy and Infectious Diseases (NIAID) grant 1R21AI164333 (to L.C.). **Author contributions:** A.H. performed all the 2D-gel experiments and ChIP and qPCR experiments and prepared samples for the EM experiments with the SV40 constructs. H.A. cloned the telomeric repeats in the pML113 vector. G.M. and M.G. performed the EM spreading and acquisition with the pTelN and pCtrl samples. G.M. performed the experiments with the mouse B cell lymphoma line. V.P. and S.C. generated the mouse B cell lymphoma cell line used for telomere enrichment and assisted with the experimental design in using this cell line. L.C. provided the *hTERT* and *hTR-TSQ1* constructs and assisted with the experimental design and analysis involving those constructs. Y.D. conceived the study, designed the experiments, and wrote the manuscript. **Competing interests:** The authors declare that they have no competing interests. **Data and materials availability:** All data needed to evaluate the conclusions in the paper are present in the paper and/or the Supplementary Materials.

Submitted 5 October 2022
Accepted 23 February 2023
Published 22 March 2023
10.1126/sciadv.adf2011